EUV Mask Defect Inspection for the 3nm Technology Node

Yannick Hermans*[a], Tilmann Heil[b], Renzo Capelli[c], Bartholomaeus Szafranek[b], Daniel Rhinow[b], Gerson Mette[b], Patrick Salg[b], Christian Felix Hermanns[b], Bappaditya Dey[a], Luc Halipre[a], Darko Trivkovic[a], Paulina Rincon Delgadillo[a], Thomas Marschner[a], Sandip Halder[a]
[a]imec, Kapeldreef 75, Heverlee 3001, Belgium; [b]Carl Zeiss SMT GmbH, Industriestraße 1, 64380 Roßdorf, HE, Germany; [c]Carl Zeiss SMT GmbH, Rudolf-Eber-Straße 2, 73447 Oberkochen, BW, Germany

ABSTRACT

The paradigm switch to a reflective mask design for EUV lithography has proven to be challenging. Within the Horizon2020 PIn3S program Zeiss and imec are collaborating to address some of these challenges. In this work, an EUV mask with a collection of programmed defects representative for the 3nm technology node was reviewed. Defect printability at wafer level was analyzed after exposure on the ASML NXE:3400B by SEM. Furthermore, the mask was analyzed on the Zeiss AIMS® EUV platform and by SEM. For P36 (1x) 1:1 L/S programmed extrusions we have demonstrated that AIMS® EUV can be used to predict ADI local defect widths as well as (µ)bridge printability. Moreover, from P36 to P32 the mask spec regarding allowed opaque L/S extrusion widths needs to be tighter considering an earlier onset of ADI (µ)bridge printability and a stronger than expected ADI defect width increase through pitch.

Keywords: 3nm technology node, EUV lithography, Defectivity, Mask review, CDSEM, Wafer print, Zeiss AIMS® EUV

1. INTRODUCTION

Reflective mask development for EUV lithography has proven to be challenging: increasing feature density, smaller feature size, a wide range of absorber materials and the need for multilayer mirror-blanks are just a few of the challenges that come with EUV masks. With these challenges mask defect and variability management also become more stringent. A series of research works have for instance shown how mask variations can contribute to stochastic defect printing as well as wafer edge placement errors in defocus.[1–4]

A way to systematically investigate mask defect detectability, repairability and wafer printability for a particular feature is through a series of intentionally placed programmed defects with increasing size. The defect printability and defect width for after development inspection (ADI) and for after development inspection (AEI) can be verified using critical dimension secondary electron microscopy (CDSEM). For instance, Das et al. found for a set of programmed opaque P32 (1x scale) line/space (L/S) mask defects that defect size increases for AEI CDSEM compared to ADI CDSEM.[5] Moreover, below a programmed defect size of about 100 nm[2], AEI CDSEM showed that the size of the defect print was subject to variation and did not even print all the time.

Besides performing CDSEM measurements on wafer prints, programmed defects can be assessed using actinic mask disposition tools which do not require the use of a lithography scanner.[6] Actinic mask disposition allows to establish an aerial image of specific mask regions by using an illuminator equivalent to that of a lithography scanner and projection optics that allows the magnification of the aerial image onto a CCD camera. The Zeiss AIMS® tools are widely used in industry for actinic defect disposition after mask patterning to identify killer defects.[7] After those defects are repaired the Zeiss AIMS® tool can be used to determine the quality of the repair. In recent work, the Zeiss AIMS® EUV was successfully used to qualify the effective repair of programmed 2.25 nm (1x) extrusions for a P44 L/S 1:1 pattern.[8] Despite the effective repair, it was not clear whether that extrusion would have led to a defect at wafer level and whether repair was needed after all.

* yannick.hermans@imec.be

38th European Mask and Lithography Conference (EMLC 2023), edited by
Uwe F.W. Behringer, Jo Finders, Proc. of SPIE Vol. 12802, 128020H
 · 0277-786X · doi: 10.1117/12.2678392

In this work, we have addressed for P36 (1x scale) 1:1 L/S to what extent opaque programmed (internal) extrusions can be detected and from which size they start to print on wafer. With AIMS® EUV, we have established that extrusions down to a width of 1.25 nm (1x) could be detected. Furthermore, the EUV programmed defect mask was exposed with the ASML NXE:3400B (0.33 NA) using an SOC/SOG/CAR resist stack to determine the defect printability and local CD of the programmed extrusions at wafer level with ADI CDSEM. We have shown that (µ)bridges do not print for extrusion widths of 1.75 nm and below and that at 1.75 nm the local CD deviates on average 11.5% from target. Moreover, a good correlation could be found between the ADI local CD and AIMS® local CD, allowing to predict from AIMS® measurements alone whether a particular opaque P36 L/S mask defect would print µbridges on wafer and what local ADI CD could be expected. Additionally, ADI CDSEM measurements for P34 1:1 L/S and P32 1:1 L/S showed that the onset of (µ)bridge printing takes place at smaller extrusion widths and that the relative local CD deviation at the programmed defect width increases stronger than what could be expected from the pitch decrease. Thus, the mask spec regarding allowed opaque defect widths needs to be tighter for lower L/S pitches.

2. METHODOLOGY

For this study a programmed defect mask has been designed and manufactured in the framework of the EU ECSEL PIn3S project, therefore the mask is called "PIn3S mask" in the following. This mask contains among others P32 to P36 1:1 vertical (vL/S) and horizontal (hL/S line/space defects as well as P45 orthogonal contact hole (oCH) defects. Mask SEM review was done on a Zeiss MeRiT LE repair tool to image the defects at mask level. The aerial image intensity at a subset of programmed defect locations was probed using AIMS® EUV measurements. The experimental setup as well as the capabilities of AIMS® EUV have been described elsewhere.[9] A horizontal dipole, vertical dipole and a quasar (Figure 1a) were used as sources during the AIMS® EUV measurements of the vL/S, hL/S and oCH programmed defects, respectively. The local CD at the programmed defects was evaluated from the AIMS® EUV aerial image maps by determining an aerial image intensity threshold based on the target CDs, being 18 nm, 17 nm and 16 nm for the P36, P34 and P32 L/S patterns.

The mask was also used for wafer prints using the ASML EUV NXE:3400B scanner. A horizontal dipole, vertical dipole and an annular (Figure 1b) flexray source were used for the EUV lithography wafer prints. The target CDs were 18 nm, 17 nm and 16 nm for the P36, P34 and P32 L/S patterns, and 32 nm for the oCH pattern. EUV compatible SOC/SOG/CAR resist thin film stacks were used during the wafer prints. ADI CDSEM was carried out on the printed wafers using the Hitachi CG5000. To study the ADI defectivity and local CD at the L/S programmed extrusions (Figure 1c) there were 984 CDSEM measurements (Figure 1d) for which the space CD at the programmed defect (MP1) as well as the neighboring space CDs (MP2-MP19) were measured (Figure 1e).

3. RESULTS

3.1 PIn3S programmed defect mask review

As a first part of this work a set of programmed P36 vL/S, P36 hL/S and P45 oCH programmed defects were studied using mask SEM, AIMS® EUV and ADI CDSEM. Many of the studied programmed defects had relatively large sizes as can be seen from the 1x design dimensions of the examples in Figure 2. Consequently, these defects could be readily distinguished in mask SEM images and AIMS® EUV aerial image maps. Moreover, ADI CDSEM images showed that these large size programmed defects systematically printed on wafer. The main aim of studying these systematic defects is to verify the success of a mask repair process, which is part of the mask repair work package of the PIn3S project and will be reported at a later stage.

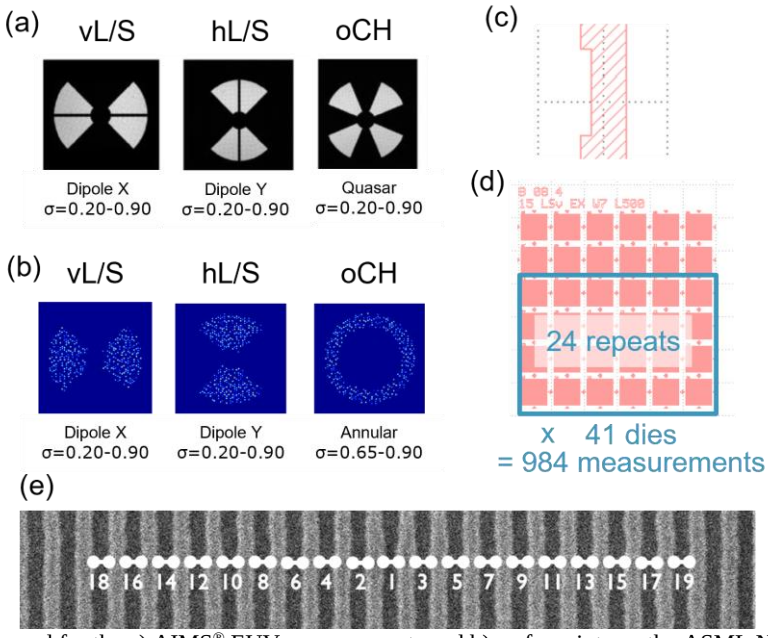

Figure 1: Sources used for the a) AIMS® EUV measurements and b) wafer prints on the ASML NXE:3400B for vertical line/spaces (vL/S), horizontal line/spaces (hL/S) and octahedral contact holes (oCH). (c) Example of a programmed extrusion on the PIn3S programmed defectivity mask. (d) ADI CDSEM measurement series for one programmed defect. (e) All local space ADI CDSEM measurement points (MP) with MP1 being the location of the programmed defect.

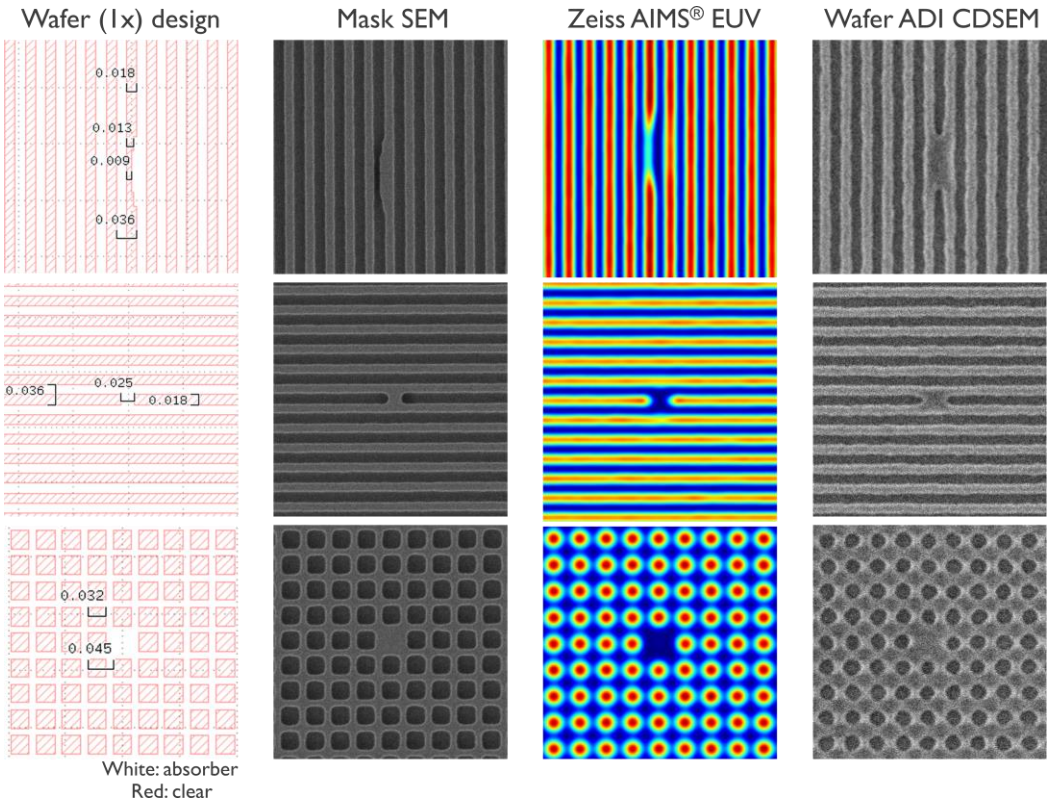

Figure 2: Examples of programmed defects for P36 vertical L/S, P36 horizontal L/S and P45 octahedral contact holes which print systematically on wafer. The programmed defects were analyzed using mask SEM, AIMS® EUV, and wafer print ADI CDSEM.

3.2 P36 L/S programmed (internal) extrusion detection and printability

As the programmed defect dimensions decrease, the ADI CD deviation as well as the likelihood of visible defectivity after ADI decreases.[5] To systematically study the printability of small L/S P36 programmed defects, a set of programmed extrusions (EX) and internal extrusions (EXI) with varying width and length (Figure 3) were measured using AIMS® EUV and ADI CDSEM. From the AIMS® EUV aerial image maps (Figure 4) all the programmed extrusions under study down to a 1x width of 1.25 nm gave rise to a considerable decrease in local aerial image intensity, allowing for their detection.

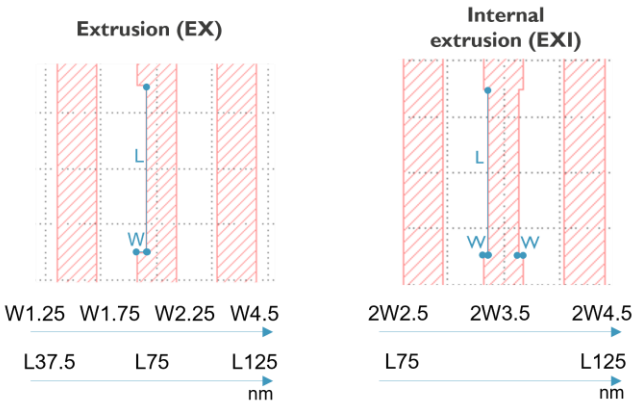

Figure 3: Series of programmed P36 L/S extrusions (EX) and internal extrusions (EXI). The total width (W (extrusions), 2W (internal extrusions)) and length (L) of the probed defects are illustrated.

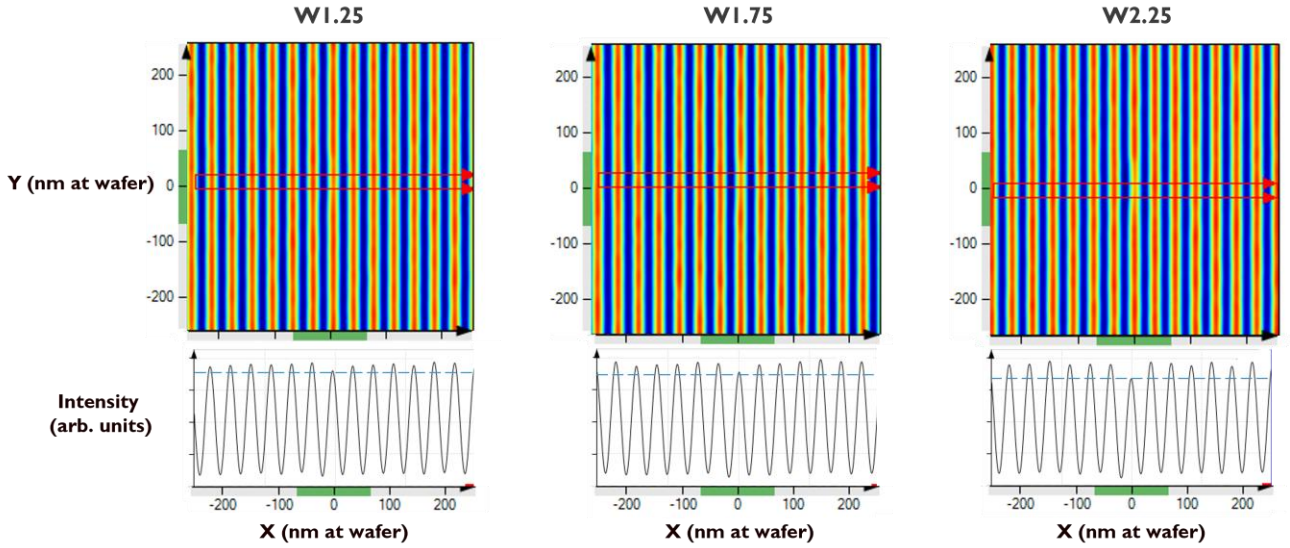

Figure 4: AIMS® EUV measurements for programmed P36 L/S extrusions with 75 nm length and various width. The upper graphs show the areal image intensity maps around the programmed extrusions. The lower graphs are plots of the aerial image intensity along the x-axis defined by the red arrows. The programmed extrusions situate at about (x: 0 nm, y: 0 nm).

The programmed mask extrusions were also further studied using wafer print ADI CDSEM in which the space CD at the local defect (measurement point 1 (MP1)) was compared to the space CD of the neighboring measurement points (MP2 to MP 19) (Figure 5). From W1.25 to W4.5 the boxplots, visualizing the CD distributions per MP, show that only the CD of MP1 was clearly affected by the programmed defect situated at MP1. Moreover, at a programmed defect width of 4.5 nm a tail of high CD outliers could be noticed for MP1. These outliers originate from faulty CD measurements caused by

bridging. Indeed, the MP1 CD scatter plot distributions in Figure 6 show that almost all the high CD outliers for W4.5 are colored red, which is used here to indicate visible (µ)bridges. For the programmed extrusions with a width of 1.75 nm and below, no visible µbridges (of 984 CDSEM images taken) could be detected. Moreover, for W2.25 only one µbridge could be detected for L75 and L125.

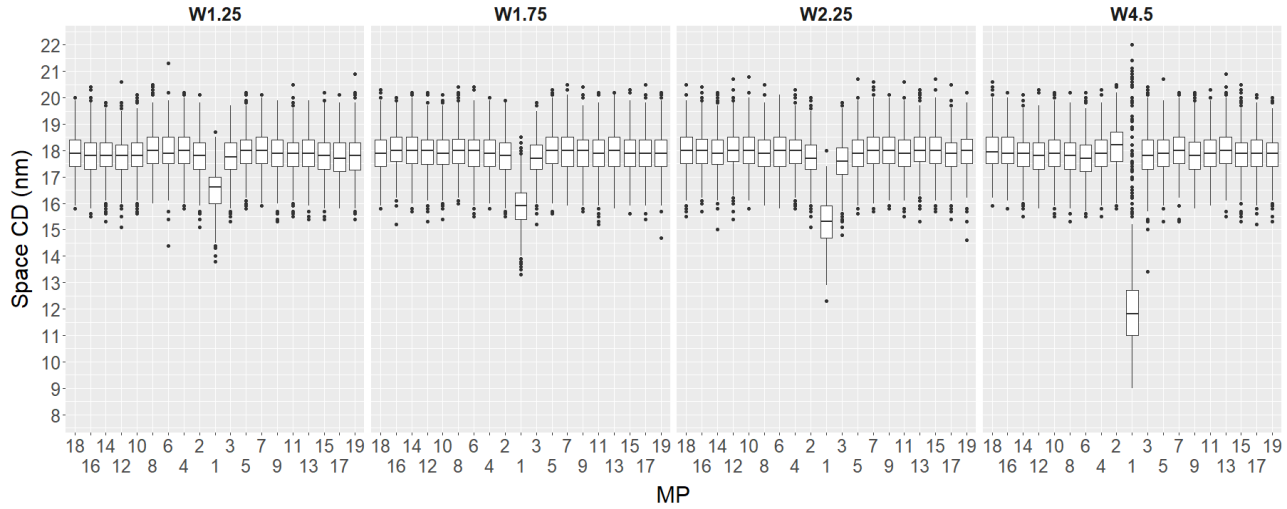

Figure 5: Wafer ADI CDSEM space CD boxplots for programmed P36 L/S extrusions with 75 nm length and various width. MP1 corresponds to the location of the programmed defect while the other MPs represent the neighboring spaces.

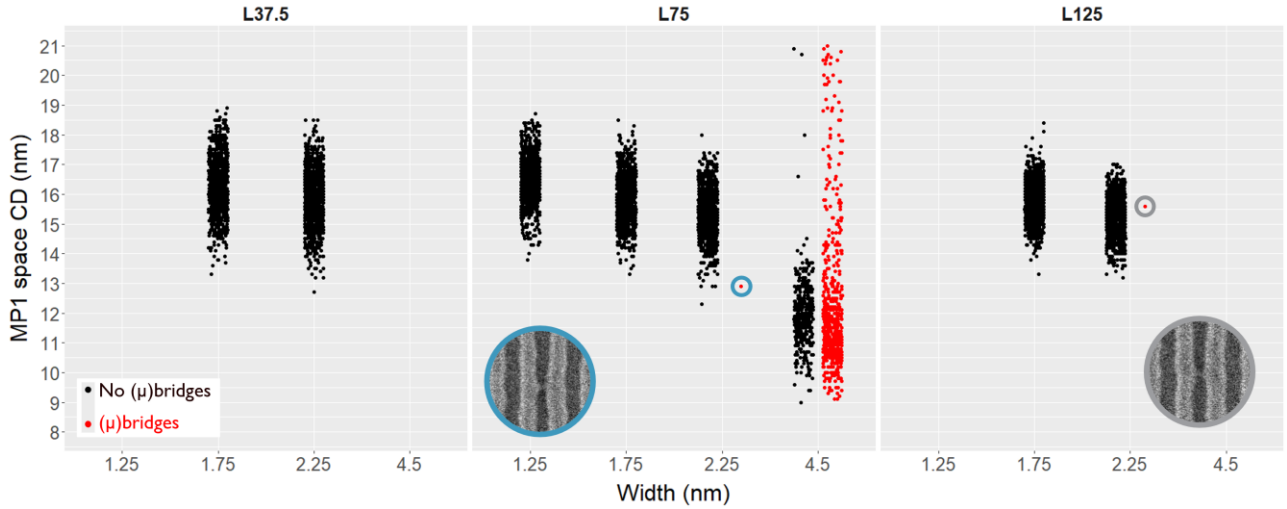

Figure 6: Wafer ADI CDSEM MP1 space CD scatter plots for programmed P36 L/S extrusions (EX) with various length and various width. Every point represents one measurement. The distributions are split based on whether a (µ)bridge could be seen at the MP1 programmed defect (red) or not (black). For some measurement points the ADI CDSEM image is shown.

For the programmed internal extrusions, the onset of µbridges lies at a total width of 2.5 nm, as a µbridge could be observed for internal extrusion lengths of 75 nm and 125 nm (Figure 7). Although a single opaque defect of 1.25 nm would not give rise to a (µ)bridge, two neighboring µbridges would. The internal extrusion CD scatterplots also show that the likelihood of a (µ)bridge rises when the length of the programmed defect increases. As such, increasing the programmed defect length could potentially be a way to test with fewer CDSEM measurements whether a programmed defect prints systematically in a particular lithography process.

For the P36 EX and EXI L/S programmed defects, Figure 8 shows a correlation of the AIMS® EUV space CD and the average ADI CDSEM CD with a slope of 1 and an offset of about 0.5 nm. This correlation allows for a reliable

prediction of the average ADI CDSEM CD and number of ADI (µ)bridges based on AIMS® EUV measurements, on the condition that a calibration curve as in Figure 8 is available. Roughly, three zones can be established based on ADI CD deviation and (µ)bridge printing. There's a green zone where the average MP1 ADI CD deviation amounts to about 2 nm and where no (µ)bridges could be identified. Then, in the orange zone the average CD deviation is smaller than 3.5 nm and 1 to 10 µbridges could be seen. Last there is a red zone with CD deviations larger than 3.5 nm and more than 10 (µ)bridges. Importantly, despite AIMS® EUV being able to detect the defects in the green zone, those defects likely do not require a repair, raising another advantage of knowing how a series of programmed defects propagate after lithography wafer prints.

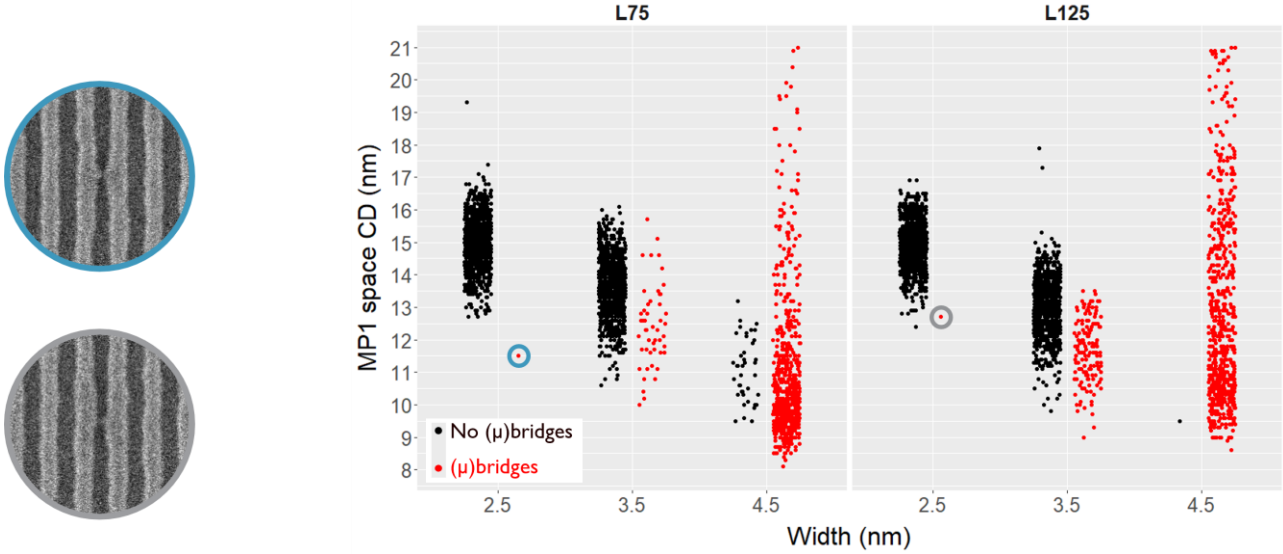

Figure 7: Wafer ADI CDSEM MP1 space CD scatter plots for programmed P36 L/S internal extrusions (EXI) with various length and various width. Every point represents one measurement. The distributions are split based on whether a (µ)bridge could be seen at the MP1 programmed defect location (red) or not (black). For some measurement points the ADI CDSEM image is shown.

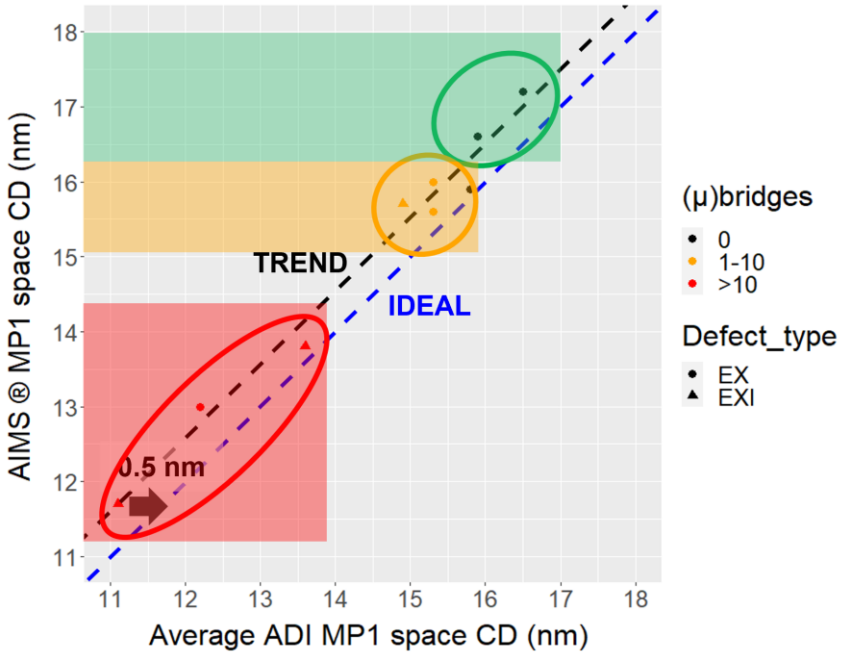

Figure 8: AIMS® EUV MP1 space CD versus average ADI CDSEM MP1 space CD. Green zone depicts the absence of (µ)bridges, yellow zone corresponds to 1-10 µbridges and the red zone represents the programmed extrusions with more than 10 µbridges.

3.3 P34, P32 L/S programmed (internal) extrusion printability

The study into the limits of (internal) extrusion L/S printability was also extended to P34 and P32. The boxplot ADI space CD boxplots for P34 and P32 (Figure 9) also show that the effect of the programmed extrusions on MPs other than MP1 is limited. Furthermore, at P32 the high CD outlier tail can now already be observed at W2.25. The ADI space CD distributions through pitch (Figure 10) show that the onset of (µ)bridges happens at earlier programmed defect widths as the pitch becomes smaller. Indeed, while for P34 and P36 (µ)bridges do not print at programmed extrusion widths of 1.25 nm and 1.75 nm (Figure 11), (µ)bridges already appear from 1.25 nm onwards for P32. Furthermore, the average ADI MP1 space CD for the same mask programmed defect width increases with decreasing pitch and more rapidly than what can be expected from the decrease in target CD through pitch. This observation can be more clearly deduced from the relative average ADI CD deviation (ΔCD/CD) versus relative programmed defect width plot in Figure 12. Figure 12 clearly summarizes that the relative CD deviation increases (e.g. for W1.25 from 8% to 11%) as the L/S pitch decreases from P36 to P32. This shows, together with the earlier onset of (µ)bridge printing, that mask specs regarding allowed mask defect sizes should tighten when going from P36 to P32 L/S.

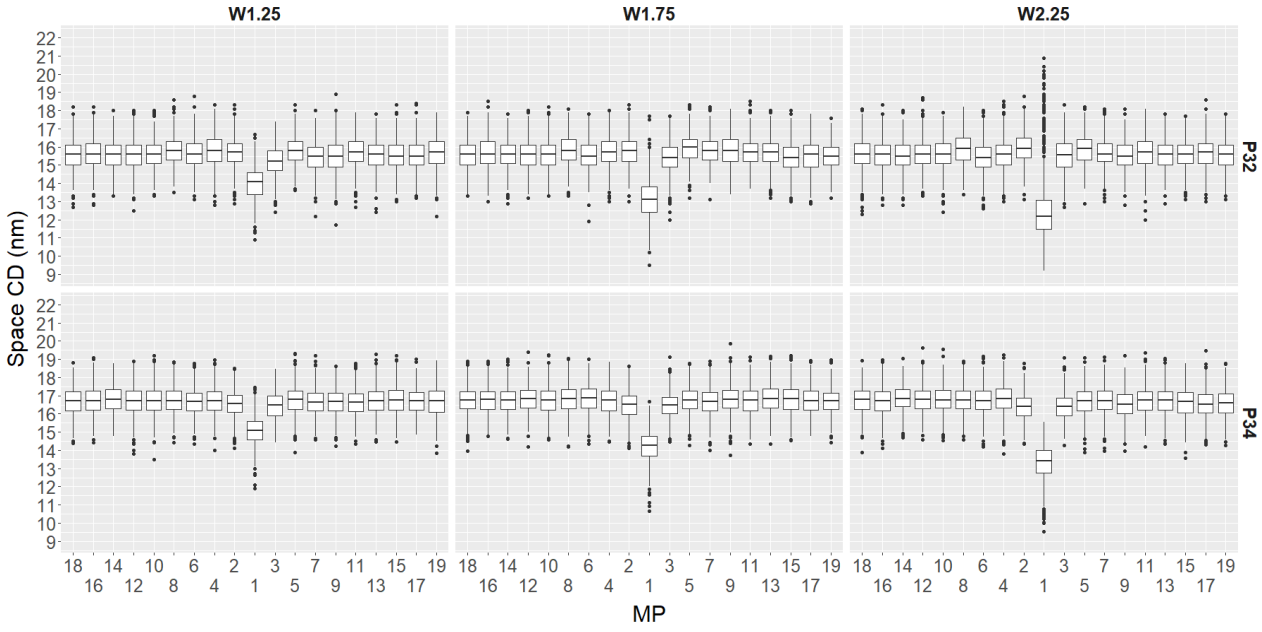

Figure 9: Wafer ADI CDSEM space CD boxplots for programmed P34 and P32 L/S extrusions with 75 nm length and various width. MP1 corresponds to the location of the programmed defect while the other MPs represent the neighboring spaces.

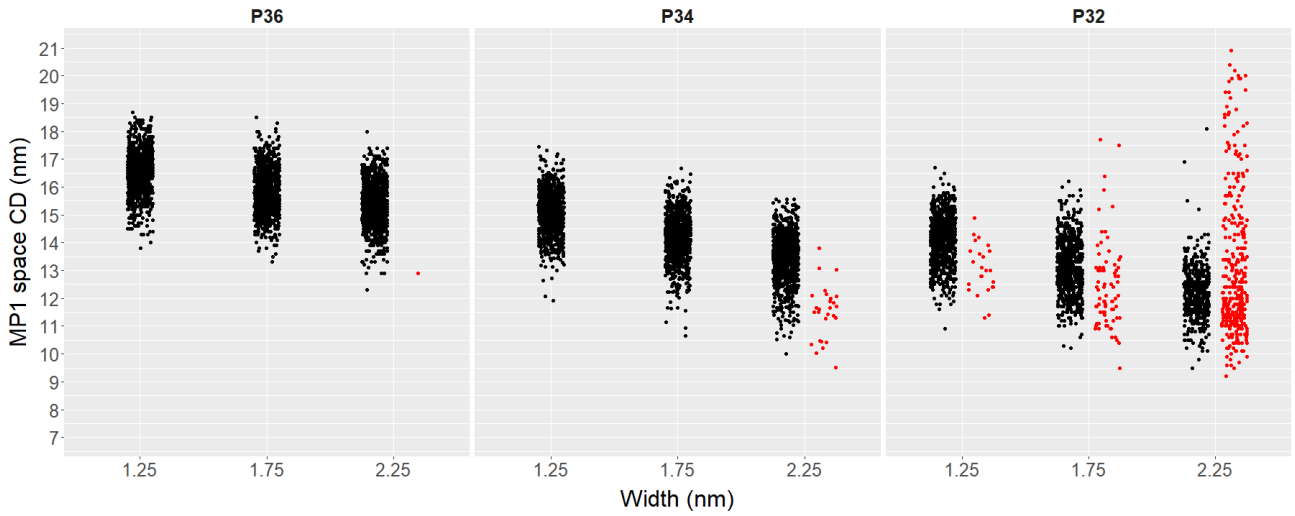

Figure 10: Wafer ADI CDSEM MP1 space CD scatter plots for programmed P36, P34 and P32 L/S extrusions (EX) with various length and various width. Every point represents one measurement. The distributions are split based on whether a (µ)bridge could be seen at the MP1 programmed defect location (red) or not (black).

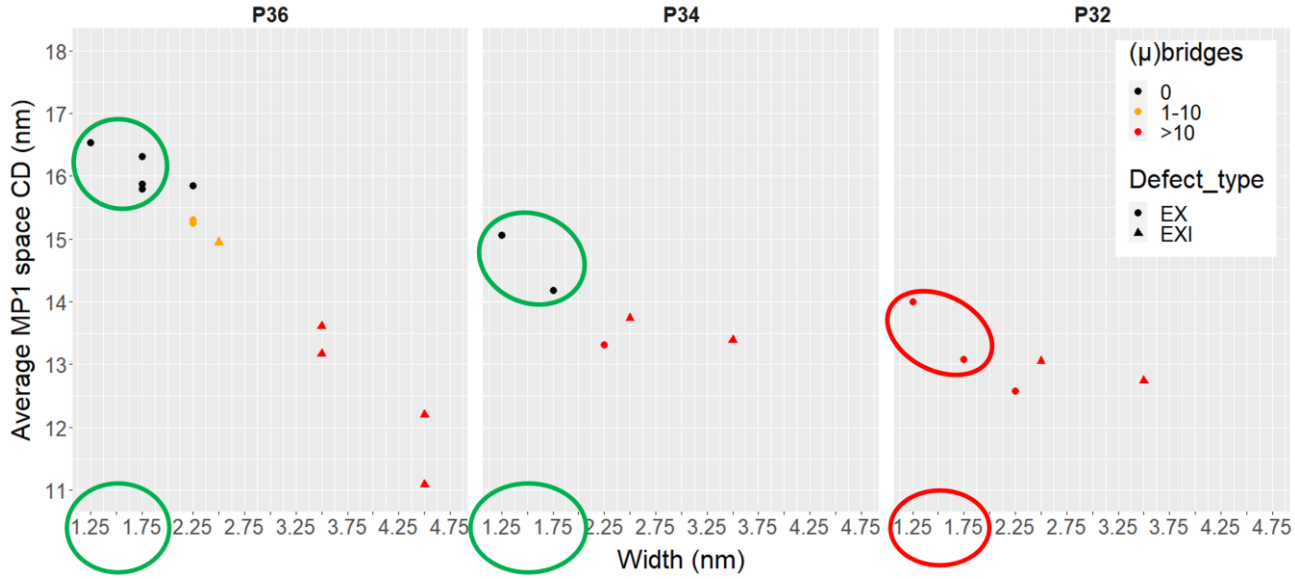

Figure 11: Average wafer ADI CDSEM MP1 space CD scatter plots for programmed P36, P34, P32 L/S extrusions (EXI) with various length and various width. Every point represents one measurement. The distributions are split based on whether a (µ)bridge could be seen at the MP1 programmed defect location (red) or not (black).

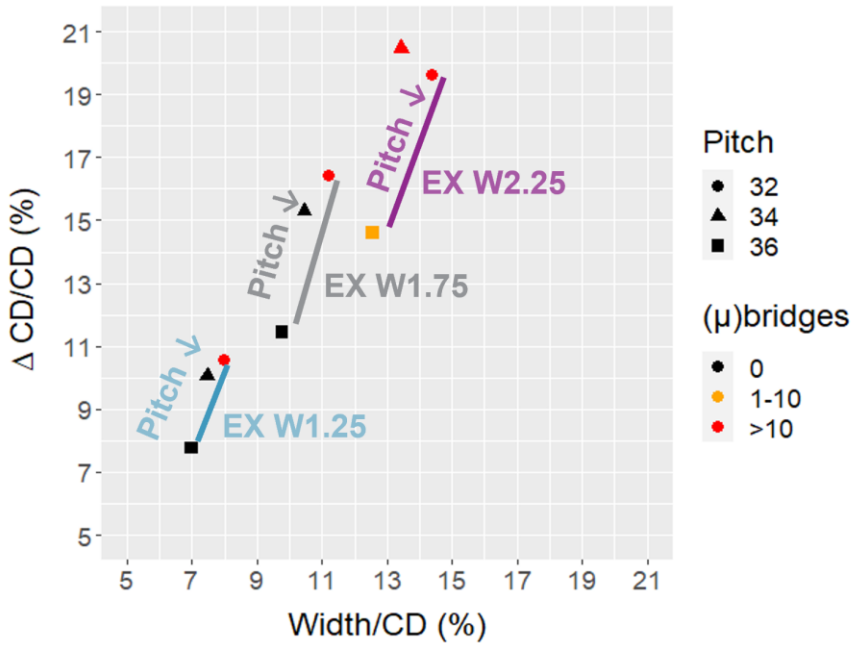

Figure 12: average ADI CDSEM MP1 ΔCD/CD (with ΔCD being MP1 CD – target CD and CD being target CD) versus relative programmed defect width/CD for extrusions with 75 nm length and various width.

4. CONCLUSIONS AND OUTLOOK

We have shown for P36 (1x) 1:1 L/S programmed extrusions that ADI local defect widths as well as (μ)bridge printability can be predicted using AIMS® EUV measurements if the correlation between AIMS® EUV and ADI wafer CDSEM has been established. Furthermore, ADI CDSEM inspections on P36 to P32 1:1 L/S programmed extrusions showed an earlier onset of ADI (μ)bridge printability and a stronger than expected ADI defect width increase through pitch. Consequently, the mask spec regarding allowed opaque L/S extrusion widths needs to tighten towards lower pitches.

Next, the PIn3S programmed defect mask will undergo a series of repair experiments. Then, AIMS® EUV and wafer print CDSEM are to be used to verify the quality of the repairs. Furthermore, how the programmed extrusion defect printability changes after etch should be understood better.

This project has received funding from the ECSEL Joint Undertaking (JU) under grant agreement No 826422. The JU receives support from the European Union's Horizon 2020 research and innovation program and Netherlands, Belgium, Germany, France, Romania, Israel.

REFERENCES

[1] Rik Jonckheere., "Overcoming EUV mask blank defects: what we can, and what we should," Proc.SPIE 10454, 104540M (2017).
[2] Rik Jonckheere and Lawrence S. Melvin III., "Stochastic printing behavior of non-local mask deficiencies in EUV lithography," Proc.SPIE 11517, 1151710 (2020).
[3] R. Jonckheere, D. Van den Heuvel, N. Takagi, H. Watanabe, and E. Gallagher., "Correlation of actinic blank inspection and experimental phase defect printability on NXE3x00 EUV scanner," Proc.SPIE 9422, 942216 (2015).

[4] Rik Jonckheere, Lawrence S. Melvin III, and Renzo Capelli., “Stochastic printing behavior of ML-defects on EUV mask,” Proc.SPIE 11147, 111470P (2019).
[5] Poulomi Das, Alain Moussa, Christophe Beral, Mihir Gupta, Mohamed Saib, Sandip Halder, Anne Laure Charley, and Philippe Leray., “Printability and propagation of stochastic defects through a study of defects programmed on EUV mask,” Proc.SPIE 11854, 118540Z (2021).
[6] Larissa Juschkin and Daniel C. Wack., “Source performance metrics for EUV mask inspection,” J. MicroNanopatterning Mater. Metrol. 21(2), 021204 (2022).
[7] Renzo Capelli, Nathan Wilcox, Martin Dietzel, Dirk Hellweg, Scott Chegwidden, and Joseph Rodriguez., “AIMSTM EUV first insertion into the back end of the line of a mask shop: a crucial step enabling EUV production,” Proc.SPIE 10810, 108100S, Photomask Technology 2018 (2019).
[8] Tilmann Heil, Michael Waldow, Renzo Capelli, Horst Schneider, Laura Ahmels, Fan Tu, Johannes Schöneberg, and Hubertus Marbach., “Pushing the limits of EUV mask repair: addressing sub-10 nm defects with the next generation e-beam-based mask repair tool,” J. MicroNanopatterning Mater. Metrol. 20(3), 031013 (2021).
[9] Capelli, R., Kersteen, G., Krannich, S., Koch, M., Fischer, L., Roesch, M. and Gwosch, K., “AIMS EUV evolution towards high NA: challenge definition and solutions implementation,” Opt. EUV Nanolithography XXXV 12051, 60–69, SPIE (2022).